Article

A Recent Study on Remediation of Direct Blue 15 Dye Using Halloysite Nanotubes

Shareefraza J. Ukkund [1,2], Prasad Puthiyillam [1], Ali E. Anqi [3], Syed Noeman Taqui [4], Masood Ashraf Ali [5], Usman Taqui Syed [6], Mohammed N. Alghamdi [7], Md Irfanul Haque Siddiqui [8], Hashim M. Alshehri [9], Mohammad Reza Safaei [10,11,*], Rayees Afzal Mir [12], Ashraf Elfasakhany [13], Emad M. Eed [14], Marjan Goodarzi [9,15] and Manzoore Elahi M. Soudagar [16]

[1] Department of Nano-Biotechnology, College of Engineering and Technology, Srinivas University, Mangalore 574146, India; shareef@sitmng.ac.in (S.J.U.); hodnanotechsit@gmail.com (P.P.)
[2] Department of Nano Technology, Srinivas Institute of Technology, Mangalore 574143, India
[3] Department of Mechanical Engineering, College of Engineering, King Khalid University, Abha 61421, Saudi Arabia; aanqi@kku.edu.sa
[4] CSIR—Central Food Technological Research Institute, Mysore 570020, India; noemansyed89@gmail.com
[5] Department of Mechanical Engineering, College of Engineering, Prince Sattam Bin Abdulaziz University, Al Kharj 16273, Saudi Arabia; mas.ali@psau.edu.sa
[6] LAQV-REQUIMTE, Department of Chemistry, Faculty of Science and Technology, Universidade NOVA de Lisboa, 2829-516 Caparica, Portugal; s.taqui@campus.fct.unl.pt
[7] Department of Mechanical Engineering Technology, Yanbu Industrial College, Yanbu Al-Sinaiyah City 41912, Saudi Arabia; alghamdim@rcyci.edu.sa
[8] Department of Mechanical Engineering, College of Engineering, King Saud University, Riyadh 11451, Saudi Arabia; msiddiqui2.c@ksu.edu.sa
[9] Department of Mathematics, Faculty of Science, King Abdulaziz University, Jeddah 21521, Saudi Arabia; hmalshehri@kau.edu.sa (H.M.A.); mgoodarzi@lamar.edu (M.G.)
[10] Department of Mechanical Engineering, Florida International University, Miami, FL 33174, USA
[11] Department of Medical Research, China Medical University Hospital, China Medical University, Taichung 40402, Taiwan
[12] Glocal School of Agricultural Science, Glocal University, Delhi-Yamunotri Marg, Mirzapur Pole, Saharanpur District, Uttar Pradesh 247121, India; Raies.afzal@gmail.com
[13] Mechanical Engineering Department, College of Engineering, Taif University, Taif 21944, Saudi Arabia; ashr12000@yahoo.com or a.taha@tu.edu.sa
[14] Department of Clinical Laboratory Sciences, College of Applied Medical Sciences, Taif University, Taif 21944, Saudi Arabia; e.eed@tu.edu.sa
[15] Mechanical Engineering Department, Lamar University, Beaumont, TX 77706, USA
[16] Department of Mechanical Engineering, Glocal University, Delhi-Yamunotri Marg, SH-57, Mirzapur Pole, Saharanpur District, Uttar Pradesh-247121, India; me.soudagar@gmail.com
* Correspondence: msafaei@fiu.edu; Tel.: +1-502-657-9981

Abstract: A set of lab-scale experiments were designed and conducted to remedy Direct Blue 15 (DB15) dye using nontoxic halloysite nanotubes (HNT) with the view to be utilized in a textile industrial effluent (TIE). The DB15 adsorbed-HNT "sludge" was used as a reinforcing agent and plastic waste to fabricate the composite. To advance the knowledge and further understand the chemical phenomena associated with DB15 adsorption on HNT, different factors like pH value, adsorbate initial concentration, adsorbent dosage, and temperature on the composite were affected experimentally tested. To estimate the adsorption capacity of HNT, nine isotherm models were applied, and it was identified that the Brouers–Sotolongo adsorption isotherm model represented the best accuracy for predicting the adsorption behavior of the HNT. Likewise, the pseudo-second-order reaction was the predominant mechanism for the overall rate of the multi-step dye adsorption process. Additionally, it was demonstrated that the mass transfer during the process is diffusion-controlled, and thermodynamic assessments showed that the process is physisorption.

Keywords: remediation; Direct Blue 15; halloysite nanotubes; diffusive mass transfer; adsorption isotherm model

1. Introduction

Our previous studies successfully demonstrate a novel nutraceutical industrial spent as a new class of bio-sorbents to amputate dyes from water and industrial effluents. The resultant dye adsorbed waste as a filler material and a plastic waste to fabricate composites [1]. The ever-growing demands for textile products are by far one of the principal supporters of ecological contamination. The insatiable consumption of water in textile industries has also led to a massive water pollution problem as well [2]. This is because, in this industry, in various stages, the discharge waste contains a variety of dyes that poses a technical challenge for the treatment of water and is, of course, a threat to the environment and health of the ecosystem [3]. Accordingly, there is a need to develop innovative, efficient, and cost-effective methods to treat textile industrial effluents. Much effort has been made to utilize different techniques, including but not limited to biologcal [4], chemical [5], photo-chemical [6], and physical routes [7–9] Despite some promising results, however, they have three significant deficiencies such as (1) economically unviable, (2) production of undesirable degradation products which display more toxicity than the precursors, and (3) production of undesirable sludge.

Adsorption as a mass transfer technique offers a plausible heat transfer coefficient and feasible approach for the remediation of dyes [10]. One of the significant drawbacks of the adsorption techniques, particularly in the remediation of dyes in a textile industrial effluent, is attributed to the production of highly concentrated sludge, which leads to a disposal problem. Initiated carbon has generally been utilized for remediation of colors in the textile industries, which adds to the complexity of the process and the final cost of the products considering the need for regeneration of active carbon [11]. This is the primary driver to seek alternative approaches aiming to treat effluents with more cost-effective and environmentally benign methods.

The requirement of the quantity of adsorbent for remediation in a textile industry runs into tons of material. Thus, the process for removing dyes from the effluents obtained from textile industries should be economical and eco-friendly. To satisfy these requirements, clay minerals are most appropriate as adsorbents for the amputation of dyes from effluents. However, clay minerals need to be optimized as nanomaterials to enhance several properties targeted for specific applications [12]. Amongst many nanoclay minerals available in abundance, halloysite nanotube (HNT) finds applications in catalysis [13], cosmetics and pharmacy [14], and medicine [15]. We have selected HNT as a choice of adsorbent to suit the design of the circular economy (CE) concept for two reasons. Firstly, it has a tubular structure with functional groups on the surface and inside the pore with different chemistries, enhancing the efficiency of adsorption during the remediation process of dyes. Secondly, HNT as a reinforcement material has been extensively used to fabricate nanocomposites [16].

Azo dyes are currently banned from use in industrial and domestic sectors all over the world. However, they are being processed to produce up to 70% of dyes used in the textile industry due to their inherent properties, such as (1) simple and cost-effective synthesis in aqueous media, (2) availability of colossal choice of starting materials, (3) a wide spectrum of shades, (4) high intensity and superior fastness of the color, (5) versatility in applications on a variety of substrates and (6) energy-saving dyeing process at 60 °C when compared to boiling temperature of its counterparts [17].

DB15 is a bis azo dye utilized to dye materials such as cellulose, leather, wool, and paper. The dye is also utilized for staining biological materials and to tint cinematographic films. The use pattern for the dye in the USA is 65%, 30%, and 5% for textile dyeing, paper colorant, and other uses, respectively [18]. Despite such promising applications, there is a lack of information on using this material for remediation of DB15 by adsorption technique [19].

Considering the above literature, the primary reason for the current investigation is to advance the knowledge on remediation of DB15 by adsorption technique and design an effective technique for the remediation of DB15 from water and textile industrial

effluent (TIE). The dye adsorbed HNT generated as "sludge" is used to fabricate novel composites using waste plastic and the CE approach.

2. Materials and Methods

2.1. Materials

Halloysite nanotubes (HNT) and Direct Blue 15 (DB15) dye (C.I. = 24400; CAS registry number = 2429-74-5; chemical formula = $C_{34}H_{24}N_6Na_4O_{16}S_4$; molecular weight = 992.81) were obtained from Aldrich, India. The dye is commonly referred to as Direct Sky Blue 5B (Figure 1).
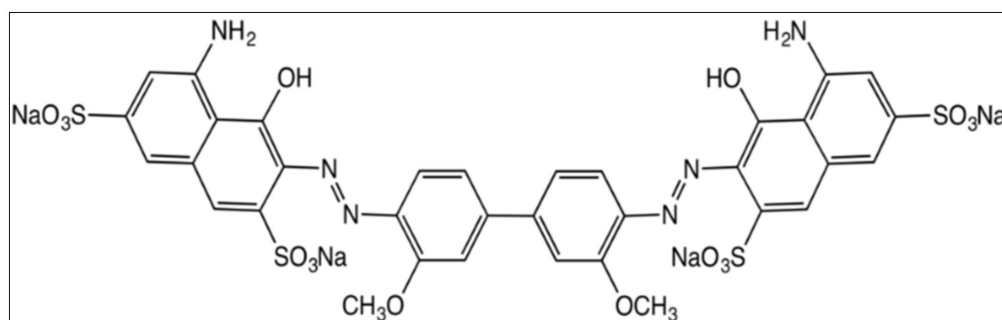
Figure 1. Structure of Direct Blue 15 dye used in the present research.

2.1.1. Investigation on Factors Effecting Adsorption of DB15 Dye on HNT

Using batch experiments, the impact of test boundaries such as pH, beginning DB15 color focus, HNT measurements, and the temperature was considered. For setting up the stock arrangement of DB15 (1000 mg L^{-1}), refined H_2O was utilized. Required arrangement focuses (25–500 mg L^{-1}) were ready from the sample. To a progression of 250 mL jars, 50 mL watery DB15 color arrangement (25–500 mg L^{-1}) was added. A necessary measure of HNT was brought into every jar. Assessments were led dependent on the impacts of fluctuating boundaries like pH (2–12), DB15 color starting concentration (25–500 mg L^{-1}), and measurements of adsorbent (0.025–0.3 g mL^{-1}; 0.5–6.0 g L^{-1}). To consider the impact of temperature on the course of adsorption, three temperatures were chosen to contemplate the underlying color convergence of 100 mg L^{-1}. The unabsorbed DB15 color in the arrangement stage was disengaged from HNT for five minutes at 3000 rpm centrifugation. In the event that the arrangement was indistinct, the centrifugation was rehashed for an extra five minutes. The DB15 color focus at balance relating to the supernatant centrifuged arrangement was settled utilizing a UV–vis spectrometer at λ_{max} 602 nm. To contemplate the impact in a scope of pH 2–12 clump tests were completed. The pH of the arrangement was adjusted using 0.01–1.00 M HCl or NaOH arrangement. Analyses were finished in three-fold and the midpoints are accounted for. The constants of variety of outcome did not surpass in all cases ±2% fault.

2.1.2. Characterization Methods

IR spectra were recorded using the FTIR spectrophotometer. The pH meter 802, manufactured by Systronics, India, was utilized to quantify pH. The point of zero charge (pHPZC) of HNT was controlled by carrying out the procedure described by us elsewhere [20,21].

2.1.3. Optimization of Process Parameters

For an adsorption process, several parameters plays vital functions in determining the dye adsorbing capacity of the adsorbent material. These include time allocated to the adsorption process, the temperature at which it is being carried out, the concentration of the adsorbate dye, the quantity of the adsorbent substance, and the pH at which the adsorption process occurs. Table 1 shows the experimental span for influencing factors

Table 1. Experimental span for influencing factors [1] (Reproduction with permission from the publisher).

| Factor	Name	Units	Minimum	Maximum
A	Time	min	0	180
B	Temp.	°C	27	50
C	Conc.	mg L^{-1}	25	500
D	Adsorbent conc.	g L^{-1}	0.500	6.000
E	pH	-	2	12

3. Results

3.1. Characterization of HNT and DB15–HNT Surfaces

Scanning Electron Microscopy and FTIR Spectrum

Surface characterization of HNT and DB15–HNT was performed via SEM. Figure 2a,b shows the surface of HNT covered with the DB15 dye. A comparison of FTIR spectra of pristine HNT, DB15 dye, and DB15 dye adsorbed on HNT revealed the following: absence of bands between 2800–3000 cm^{-1} was identified in pristine HNT (Figure 3), whereas a tiny band appeared at around 3750 cm^{-1} was ascribed to traces of adsorbed water. The typical bands around 2830 and 2852 cm^{-1} were because of C–H stretching asymmetric and symmetric vibrations, respectively. The vibration band at 1000–1080 cm^{-1} was correlated to the vibrations of single bonds of Si–O, Al–O, and C–O molecules.

FTIR spectra for DB15 dye exhibit the distinctive N–H and CH-aromatic stretching vibrations bands around 2800–3000 and 2900 cm^{-1}, respectively. The vibration around 1700 cm^{-1} was accredited to S=O of the sulfites group in dyes structure. The triplet bands generally ascribed to C=C in aromatic rings attached with N=N of the azo cluster are seen around 1640, 1570, and 1460 cm^{-1}. The multiple bands attributed to N–H and CH bending vibrations that appear at around 1460–1300 cm^{-1} were also realized.

FTIR spectra of DB15 dye showed a significant band in the range 2800–3000 cm^{-1}. This band appears to be less intense and tends to vanish due to the interactions between the NH groups in dyes with Si/Al in HNC as (Si^{4+} ⋯ :NH and Al^{3+} ⋯ :NH) in the DB15–HNT FTIR spectra. Additionally, the disappearance of the N = N stretching band around 1598 cm^{-1} confirms the adsorption of the DB15 dye on HNT. The interaction between components will affect the property of double bonds and increase the character of the single bond, which is reflected in a sharp expansion in the force of the band around 1100 cm^{-1}. Moreover, the disappearance of IR absorption frequencies established the adsorption of DB15 onto HNT. Determination of pH$_{PZC}$ confirms that HNT at pH 7.61 displays zero charges (Figure 4).
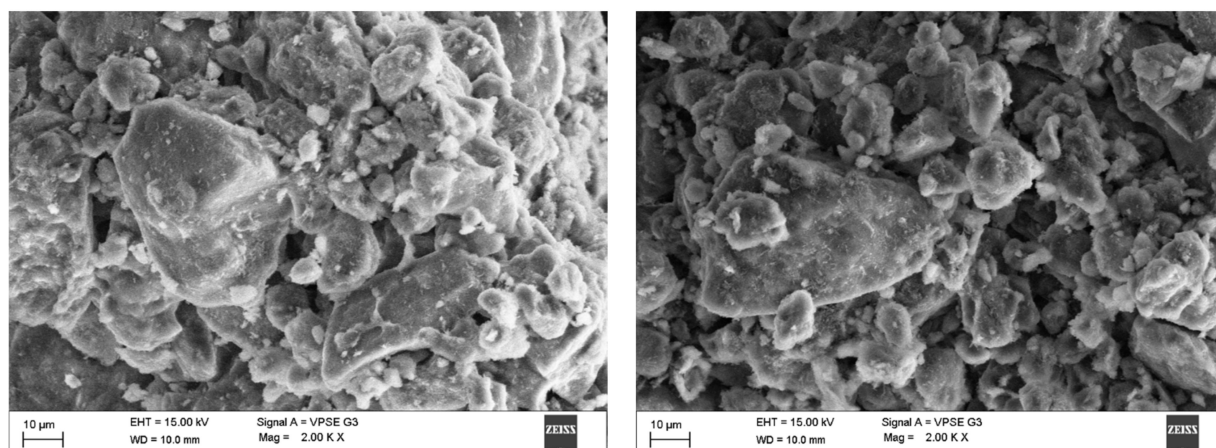
(**a**) SEM image of HNT before adsorption   (**b**) SEM image of DB15–HNT after adsorption

Figure 2. Surface characterization of halloysite nanotubes before and after adsorption studies.
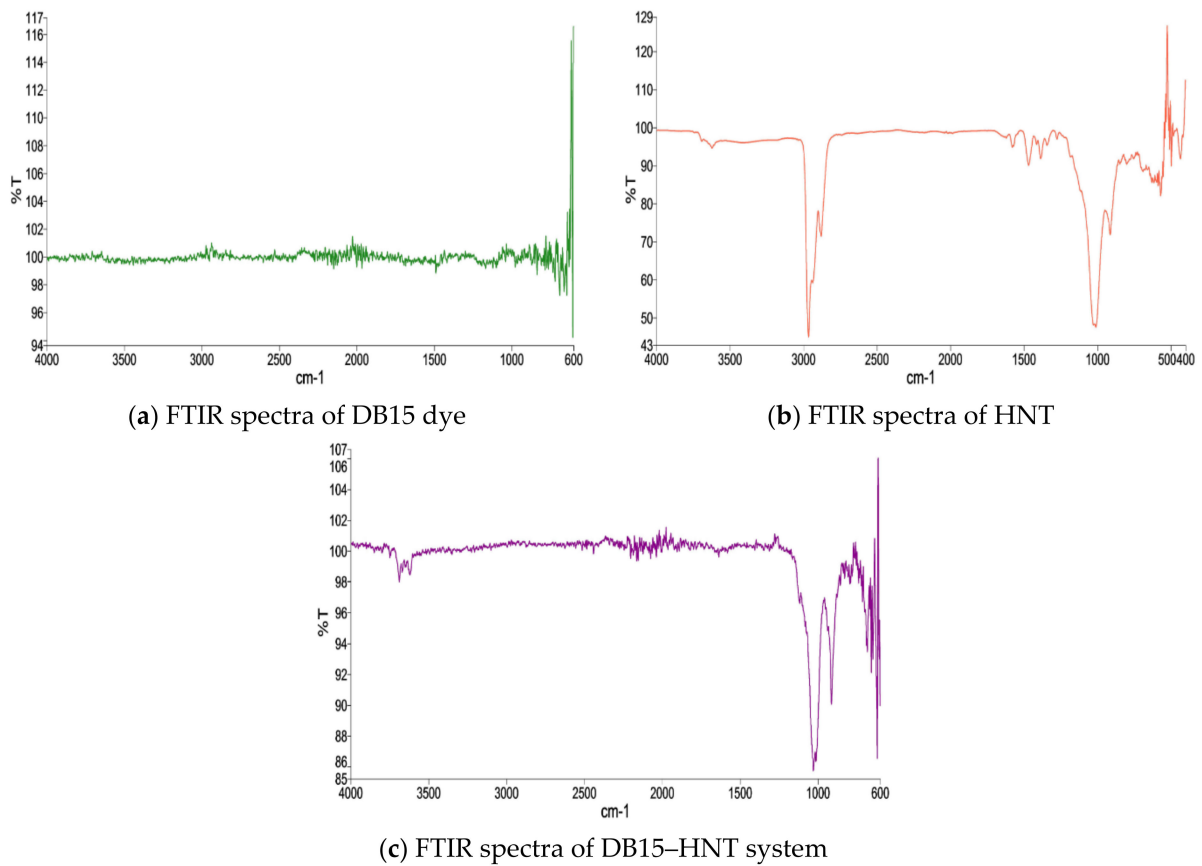
(**a**) FTIR spectra of DB15 dye

(**b**) FTIR spectra of HNT

(**c**) FTIR spectra of DB15–HNT system

Figure 3. FTIR spectra of the samples under study.
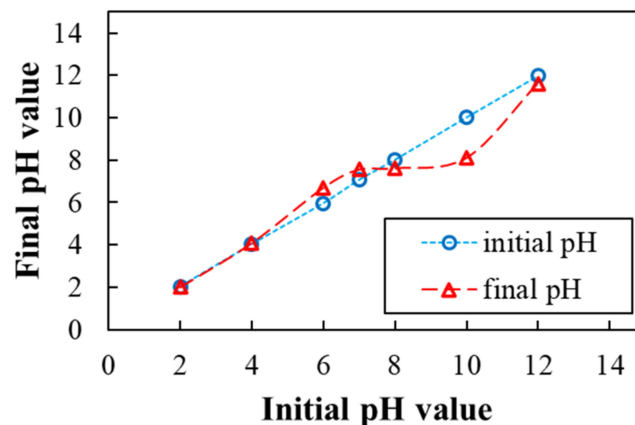
Figure 4. The deliberate mark of zero charges of HNT at the convergence.

3.2. The Impact of Factors on DB15 Adsorption on HNT

3.2.1. pH Value of Solution

The adsorption limit of HNT relies upon the value of the pH solution. The pH value majorly influences the attributes of the adsorbent surface and the chemistry of the dye solution [22]. The value of pH, reflects the efficiency of the adsorbent. This boundary is critical when the interaction is scaled too higher. Technology readiness level (TRL) and the commercial stage [23]. As depicted in Figure 5a, the shape of the curve was consistent with the expected results already published in the literature. The primary components of HNT are the oxides of Al and Si. These oxides have various ionization features and surface charges because different zeta potential rates when remained in touch with water [24]. At pH > 1.5, the external surface of HNT has negative charges due to the presence of silica

in its chemical structure (Figure 6). Conversely, at a lower pH the anionic dye exhibits a positive charge (see Figure 5a). Thus, adsorption at a higher level occurs in the pH range of 2–4. A rise is seen in the level of pH the amount of degree of protonation of NH_2 and OH groups of the dye decreases. Accordingly, the adsorption capacity of the substrate decreases sharply from pH 4 to 6. A sharp increase at pH > 10 is likely due to dye adsorption onto positively charged Al^{3+} and Si^{4+} ions. Moreover, the degradation of the dye at pH > 10, resulting in a decrease in absorbance of the experimental solution, cannot be ruled out.

3.2.2. Initial DB15 Dye Concentration

The effect of this factor has a profound impact on the adsorption capacity of HNT. This is manifested in the results displayed in Figure 5b. The nature of the curve implies that the % elimination capability of the adsorbate (DB15) by the absorbent (HNT) is maximum in the lower concentrations of the dye and declines with a surge in the concentrations, as seen in most of the cases [25]. Conversely, the q_e increases sharply from 25–200 mg L^{-1}, and a marginal rise was noticed with a rise in the conc. level.

3.2.3. Effect of Adsorbent Dosage

For example, the elimination of DB15 dye from the sample enhances with an rise in the adsorbent dosage from 0.025 to 2.0 g L^{-1}. It was noticed, the percent of DB15, the removal of the dye, grew exponentially from 0.025 to 2.0 g L^{-1} with a rise in the amount of the adsorbent dosage. Thereafter, the marginal increase in the removal efficiency was observed (see Figure 5c). This perception accepts significance in the commercialization cycle, where the quantity of preliminaries with the least measures of the adsorbent considerably builds the evacuation effectiveness of the dye by HNT.

3.2.4. Effect of Temperature

The impact of temperature on DB15 color adsorption onto HNT is introduced in Figure 5d. The information obtained for the traditional thermodynamic boundaries, specifically, $\Delta G°$, $\Delta H°$, and $\Delta S°$ show the kind of response. For instance, the +ve $\Delta H°$ values obtained from 303 to 323 K of HNT demonstrate the endothermic interaction. The −ve benefit of $\Delta G°$ for the DB15–HNT framework affirm the suddenness and feasibility of the adsorption interaction. The size of $\Delta G°$ esteems is demonstrative of quick and unconstrained adsorption at lower temperatures. Further, it is surmised that +ve upsides of $\Delta S°$ (entropy) demonstrate the homogeneity of the surface at the interface of the DB15 color and the HNT [26].
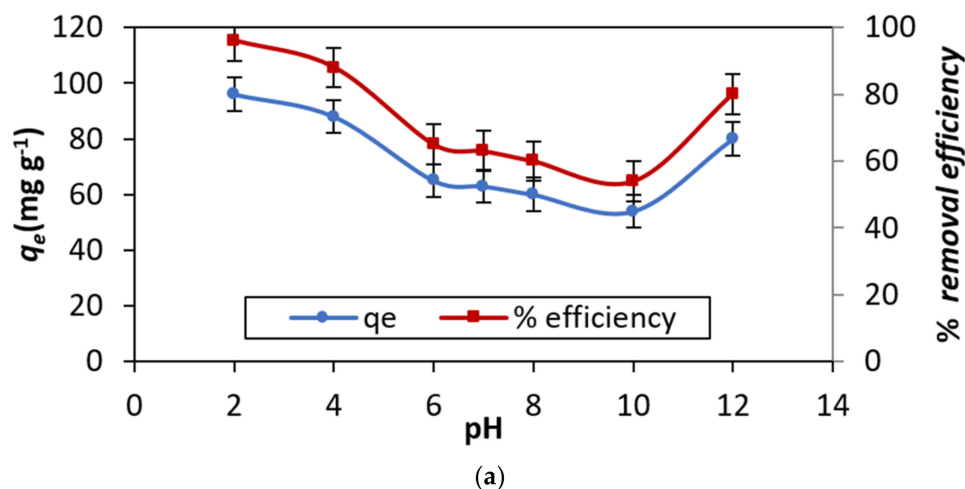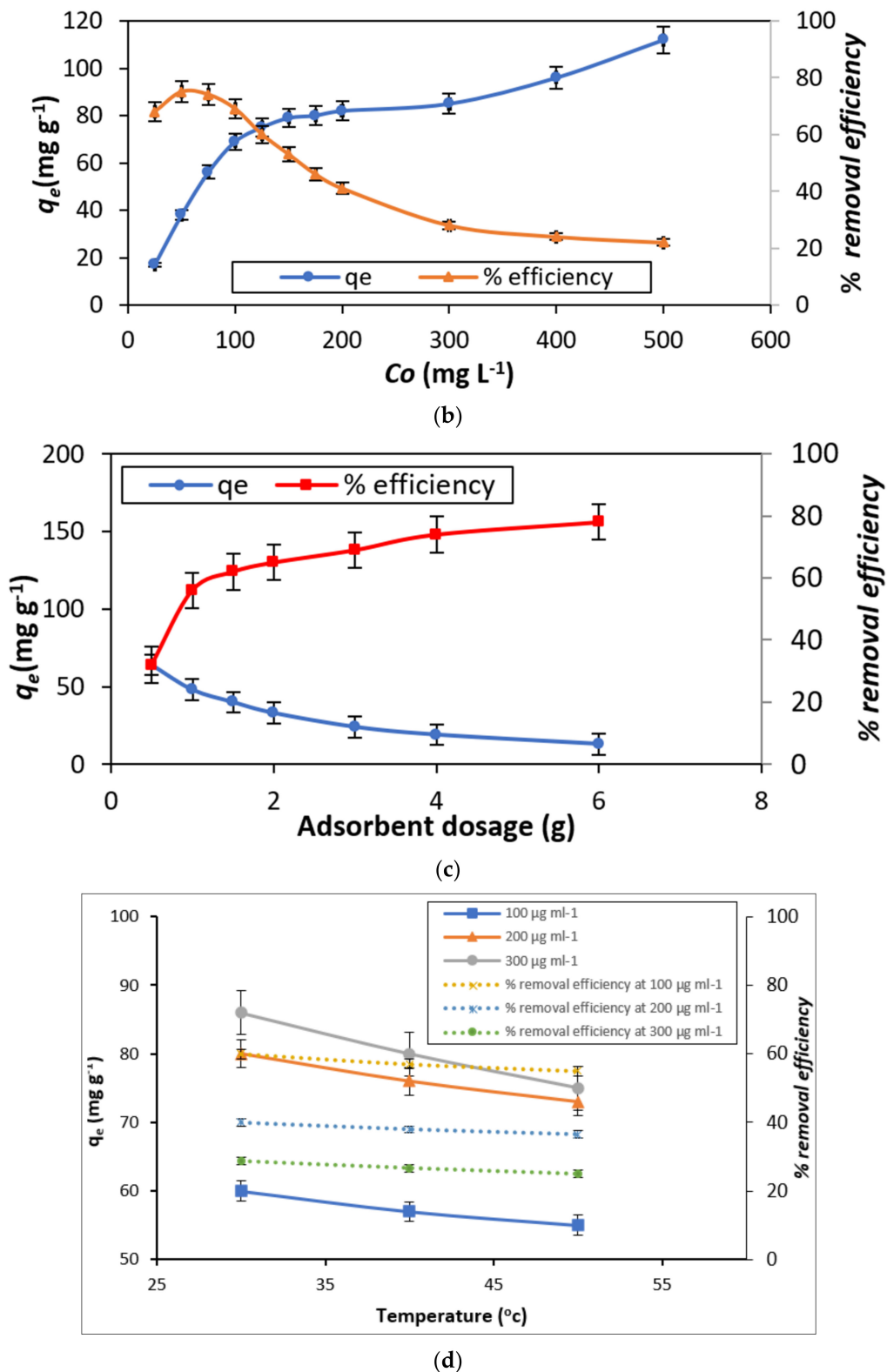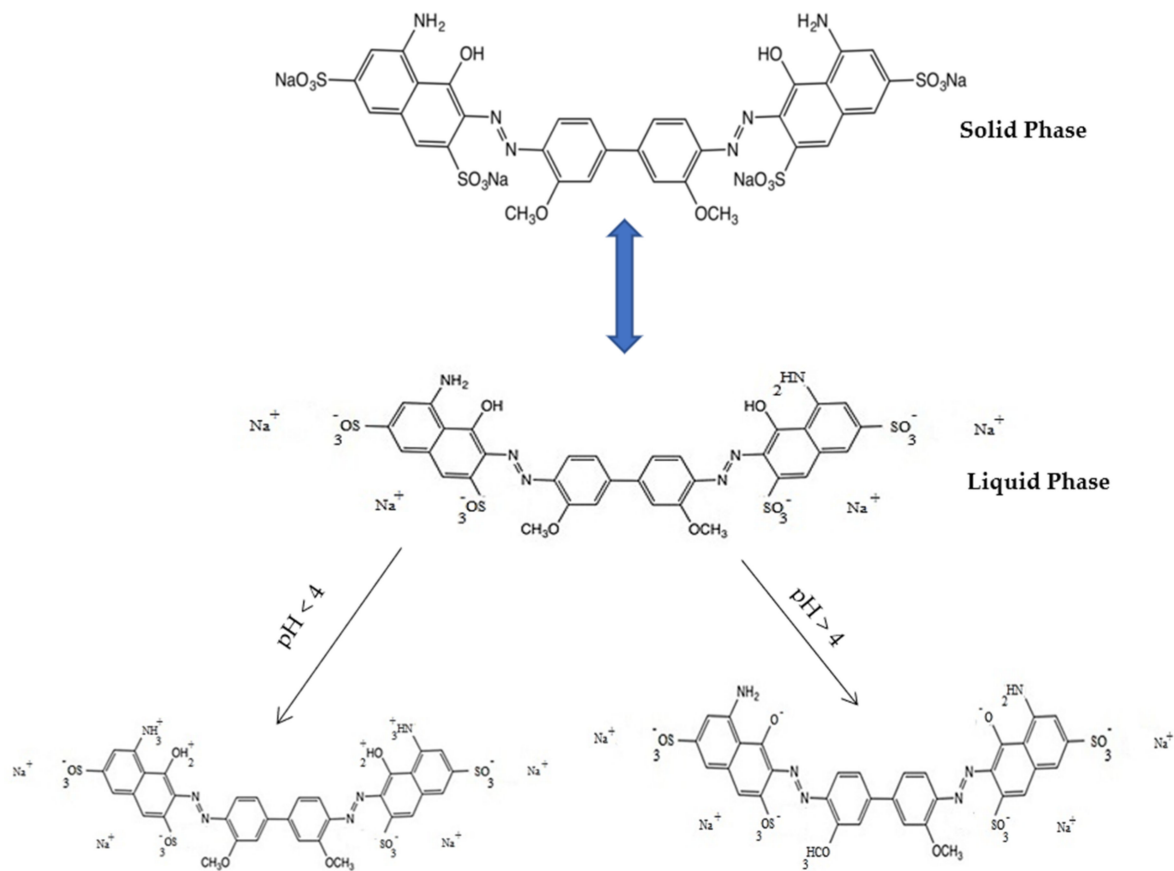

(a)

Figure 5. *Cont.*

(**b**)

(**c**)

(**d**)

Figure 5. Adsorption capacity and percentage of dye removal efficiency: (**a**) Effect of pH,(**b**) Effect of initial concentration of DB15 (adsorbate), (**c**) Effect of HNT (adsorbent) dosage, and (**d**) Effect of temperature.

Figure 6. Structures of Direct Blue 15 dye in an aqueous medium.

3.3. Adsorption Isotherms—Modeling Examination

The data of adsorption of DB15 dye by HNT were analyzed by applying the adsorption isotherm models proposed by Freundlich, Jovanovic, Dubinin-Radushkevich, Langmuir, Toth, Vieth-Sladek, Radke-Prausnitz, Redlich-Peterson and Brouers-Sotolongo, isotherm models. To refine the outcomes and to make a differentiation between practically comparable information acquired by different isotherm models, SSE and χ^2 as two extra blunder capacities were consolidated in our examination.

Langmuir [27] proposed a model in which the adsorbent was accepted to have dynamic locales having practically uniform energies. This was additionally settled on the possibility that no horizontal collaboration happens between adsorbed atoms. A level in a two-dimensional diagram with harmony focus (C_e) as a free factor and q_e (Figure 7a) as a reliant variable describes the immersion of the adsorbent's active destinations on a superficial level [28]. This suggests that further adsorption cannot happen, and the possibility of multi-facet adsorption of the color is precluded. The experimental data, $R^2 = 0.94$, $q_e = 69.00$ mg g^{-1}, and $Q_m = 97.96$ mg g^{-1} for the DB15–HNT system, indicates a good fit for the Langmuir adsorption isotherm model. The separation factor (R_L) values of 0.035 and 0.419 indicate favorable adsorption of the DB15 dye onto HNT.

In addition, the adsorption is more likely if the rise in the starting concentrations reduces the RL. This, however, goes against what is seen in Figure 7a. Furthermore, HNT has offered motivation to study different models by variations of 98.96 and 69.00 mg g^{-1}, Q_m/Q_e ratios.

The Jovanovic model [29] tries to reduce the deviancies from the Langmuir isotherm Comparing the variance in the values of $q_e = 69.00$ mg g^{-1} and $Q_m = 85.67$ mg g^{-1} with respect to Langmuir isotherm model.

The adsorption isotherm empirical model proposed by Dubinin–Radushkevich [30] describes adsorption by filling the pore of the adsorbent A value of 110.59 mg g^{-1} for q_s con-

trasts with the Langmuir and Jovanovic models (Table 2). Additionally, a value of 0.97 for the correlation coefficient (R^2) confirms that the process of adsorption is linear (Figure 7b).
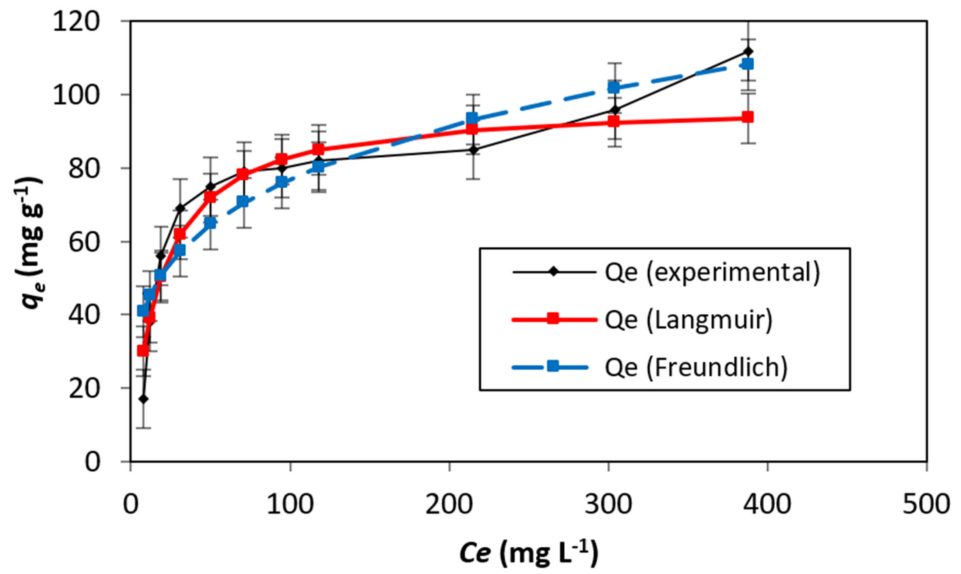
(**a**)
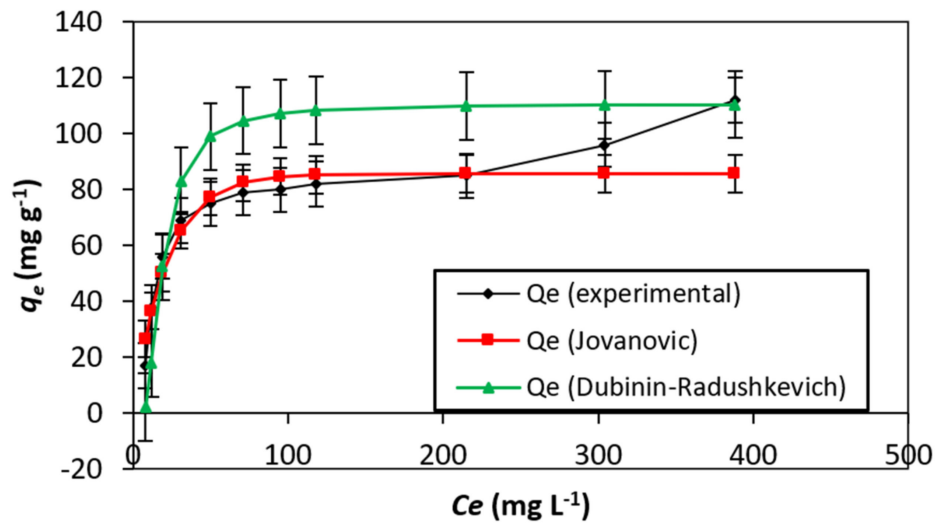
(**b**)

Figure 7. *Cont*.
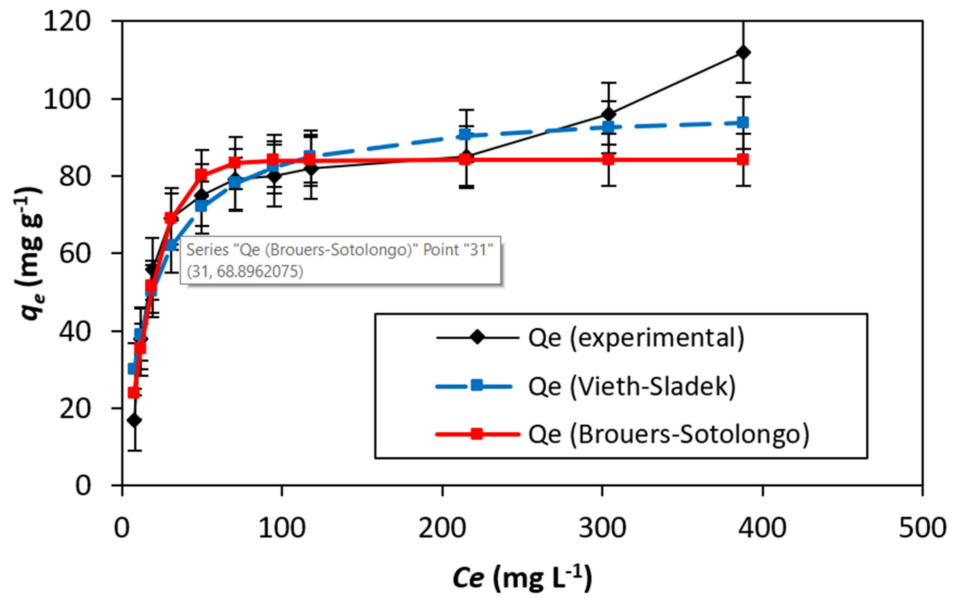
(c)
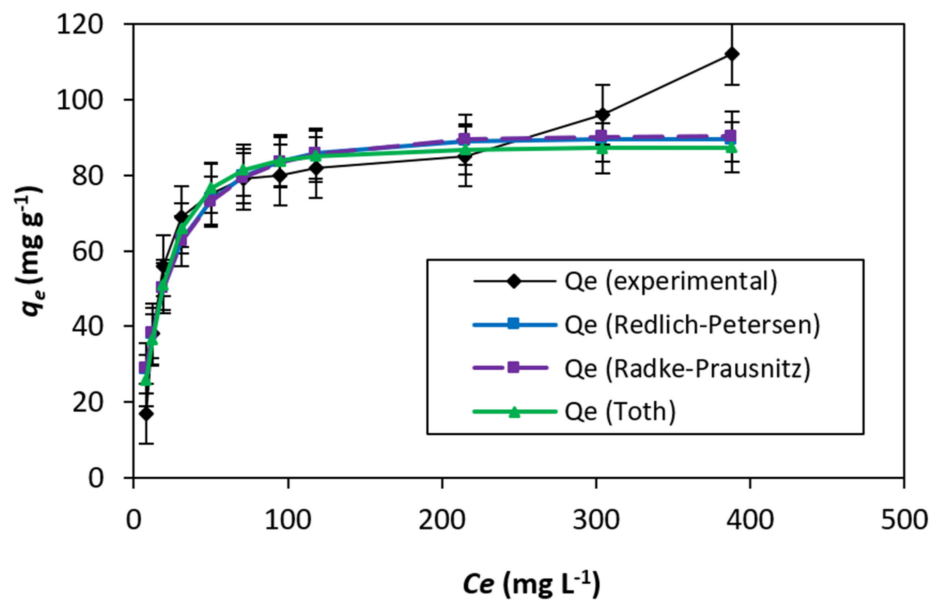
(d)

Figure 7. (**a**–**d**) The curve fitting was conducted on adsorption data isotherm for DB15–HNT.

Table 2. Two-parameter isotherms.

Two Parameter Isotherms							
Langmuir		**Freundlich**		**Jovanovic**		**Dubinin–Radushkevich**	
Q_m	**97.96**	K_F	24.17	Q_m	85.67	Q_s	110.59
K_S	0.055	n_F	3.977	K_J	0.046	K_{ad}	4.46×10^{-5}

Toth, Radke–Prausnitz, Vieth–Sladek, Redlich–Peterson, and Brouers–Sotolongo, were also studied [31]. To define a heterogeneous adsorption system, a mathematical correlation was developed by Toth [32]. Brouers–Sotolongo isotherm model [33] and the Vieth–Sladek

isotherm model [34], respectively. The results are presented in Figure 7c. Radke–Prausnitz isotherm model [35]. The Redlich–Peterson isotherm model [36], the a"*g*" value of 1.063 as a correction exponent showing similarity to the Langmuir isotherm (see Figure 7d).

　　Table 2 represents the results obtained with two-parameter isotherms, while, in Table 3, the parameters were calculated using three-parameter models. Finally, in Table 4, the curve-fitting results calculated for nine isotherm models are represented. Briefly speaking, the graphs plotted based on the nine models showed similar trends, including nonlinear and flat parts.

Table 3. Three-parameter isotherms.

Three-Parameter Isotherms									
Toth		**Brouers–Sotolongo**		**Vieth–Sladek**		**Radke–Prausnitz**		**Redlich–Peterson**	
Q_m	87.60	Q_m	84.00	A_{RP}	4.70	Q_m	114.80	A_{RP}	4.70
n_{T0}	1.876	K_{BS}	0.027	B_{RP}	0.034	K_{rp}	0.043	B_{RP}	0.034
b_{T0}	442.37	α	1.21	g	1.06	m_{rp}	1.06	g	1.06

Table 4. Results of the curve fitting for isotherm models.

| Isotherms	Langmuir	Freundlich	Jovanovic	Dubinin–Radushkevich	Toth	Brouers–Sotolongo	Vieth–Sladek	Radke–Prausnitz	Redlich–Peterson
SSE	321.3	1080.3	297.4	4324.3	227.2	281.7	321.3	306.4	296.9
χ^2	12.14	40.80	8.02	67.55	6.42	5.59	12.14	10.79	10.15
R^2	0.94	0.80	0.94	0.97	0.96	0.95	0.94	0.94	0.95

3.4. Adsorption Kinetics

　　To offer the difference in adsorption rate, the concentration of 100, 200, and 300 mg L^{-1} of the DB15 dye was utilized to carry out kinetic studies at 303, 313, and 323 K. The used kinetics limitations are given in Table 5.

Table 5. Parameters used for adsorption kinetic models in the present research.

Initial Dye Concentration [μg mL^{-1}]	Temp [K]	Pseudo-First Order					Pseudo-Second Order			
		$q_{e,expt}$ [mg g^{-1}]	$q_{e,pred}$ [mg g^{-1}]	k_1	R^2	χ^2	$q_{e,pred}$ [mg g^{-1}]	k_2	R^2	χ^2
	303	60	50.18	1.40×10^{-1}	0.68	0.96	55.64	3.99×10^{-3}	0.87	1.72
100	313	57	48.58	1.40×10^{-1}	0.63	1.10	53.92	4.10×10^{-3}	0.84	0.46
	323	55	45.89	1.54×10^{-1}	0.58	0.98	50.40	5.07×10^{-3}	0.81	0.42
	303	80	70.67	1.79×10^{-1}	0.78	0.39	75.69	4.78×10^{-3}	0.95	0.08
200	313	76	65.34	6.53×10^{1}	0.51	0.54	65.88	1.71×10^{-3}	0.76	1.65
	323	73	64.35	2.19×10^{-1}	0.51	0.54	67.94	7.39×10^{-3}	0.80	0.22
	303	86	76.28	2.39×10^{-1}	0.49	0.47	79.82	7.72×10^{-3}	0.80	0.19
300	313	80	68.28	2.97×10^{-1}	0.40	0.20	70.19	1.54×10^{-2}	0.71	0.10
	323	75	68.07	3.04×10^{-1}	0.46	0.14	69.78	1.70×10^{-2}	0.79	0.06

　　Figure 8 represents the results of the kinetic models developed for DB15. The kinetic data of adsorption of DB15 on minerals were analyzed using a pseudo-1st-order [37] and a pseudo-2nd-order [38].
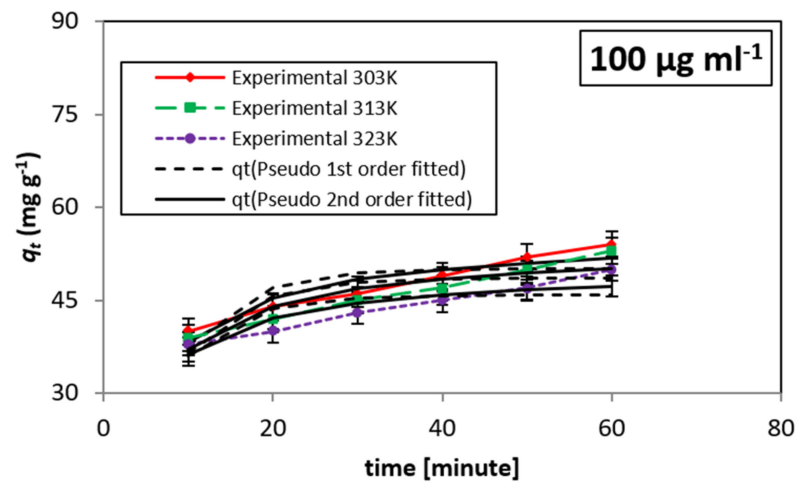
(**a**)
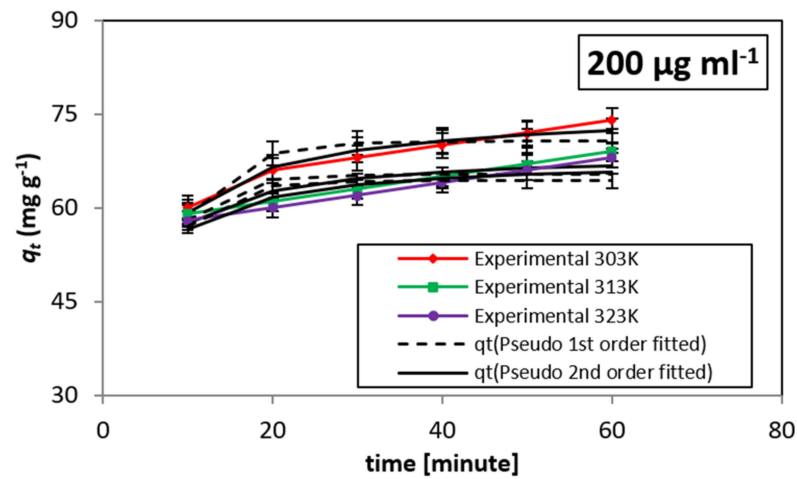
(**b**)
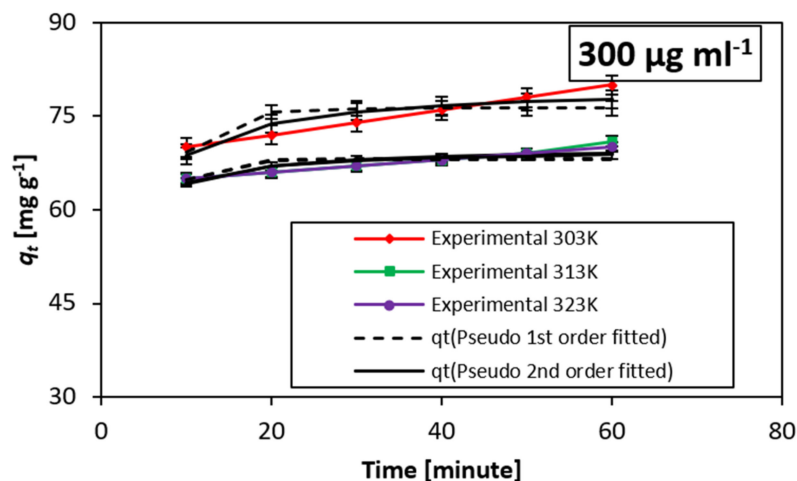
(**c**)

Figure 8. (**a**–**c**) Kinetic model developed for DB15 dye on HNT system at different temperatures.

Examination of the kinetics data (Figure 8) represents raise in adsorption with an increase in adsorbent concentration. Similarly, the adsorption rate increases with time. However, it is realized that the rate of adsorption decreases as the temperature increases.

Thus, a high concentration of adsorbent studied for a longer time interval seems more favorable for future studies.

This was observed in the film diffusion model [39]. As described in Figure 9 and Table 6, the diffusion constant R' values of a liquid film are in good agreement with high R^2 values. Furthermore, the values of R' infers, fast adsorption of solute on the atoms' exterior leaving a thin layer.
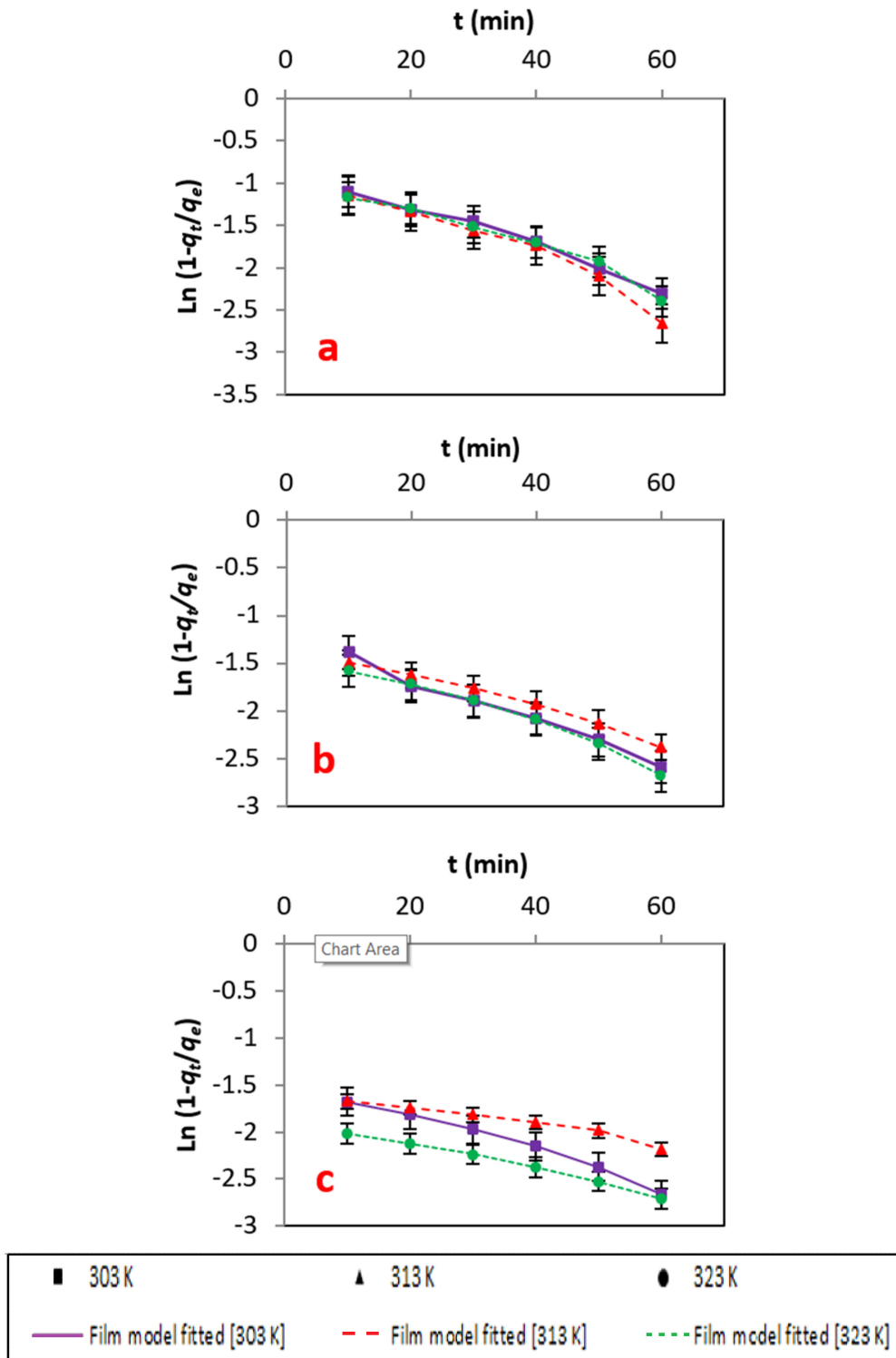

Figure 9. (**a–c**) Energy information fitted to the film diffusion model at different concentrations.

Table 6. The parameters used in the diffusion models.

Initial Dye Concentration [μg mL^{-1}]	Temp [K]	Film Diffusion Model		Weber–Morris Model		Dumwald–Wagner	
		R' [min^{-1}]	R^2	k_{id} [mg g^{-1} s$^{-0.5}$]	R^2	k [min^{-1}]	R^2
100	303	0.0238	0.98	3.05	0.99	0.021	0.98
	313	0.0285	0.94	2.99	0.98	0.026	0.93
	323	0.0234	0.95	2.59	0.98	0.021	0.94
200	303	0.0225	0.99	2.89	0.98	0.021	0.99
	313	0.0175	0.98	2.18	0.98	0.016	0.98
	323	0.0216	0.97	2.18	0.98	0.020	0.97
300	303	0.0193	0.98	2.18	0.98	0.018	0.98
	313	0.0096	0.95	1.23	0.94	0.009	0.95
	323	0.0138	0.99	1.09	0.98	0.014	0.99

3.5. Mechanistic Study

In this section, mathematical models of adsorption reaction and adsorption diffusion are proposed to identify the contribution of the diffusion mechanism in the adsorption process of the DB15 dye by HNT. Results showed that the empirical affiliation of the acceptance of the substrate at a certain time q_t is comparable with $t^{\frac{1}{2}}$. This was carried out by fitting an intra-particle diffusion model. As presented, the process of adsorption is not rate-limiting, and the development of adsorption happens in numerous stages. Thus, it may be pictured that the movement of DB15 dye molecules onto the peripheral of HNT precedes the diffusion into the pores of HNT.

For the Weber–Morris model, the solute endorsement differs with $t^{\frac{1}{2}}$, As shown in Figure 10, a straight line was obtained when plotting q_t versus $t^{\frac{1}{2}}$. Hence, it can be concluded that intraparticle diffusion is the rate-limiting step for the process of adsorption of the dye on the adsorbent [37–39]. The results of this model can be seen in Figure 11 and Table 6.

3.6. Thermodynamics of the Adsorption Process

Gibbs free energy change ($\Delta G°$) and entropy ($\Delta S°$) of the dye–HNT classification is assessed in this section as two key thermodynamic parameters. In Table 7, the calculated thermodynamic parameters are presented. The outcome of $\Delta G°$ proposes that the adsorption method is almost spontaneous. The decline in the $-^{ve}$ number of $\Delta G°$ with an increment in the temperature shows that the response is practically unconstrained at a low temp. The $+^{ve}$ upsides of $\Delta S°$ show the arbitrariness of the dye/HNT interface. Figure 12 illustrates the (a) Determination of enthalpy and Gibbs free energy: plot of thermo-dynamic equilibrium constant against 1/T and (b) Determination of activation energy: plot of pseudo-second order kinetic constant against 1/T.

Table 7. Impact of temperature and beginning color focus on thermodynamic boundaries.

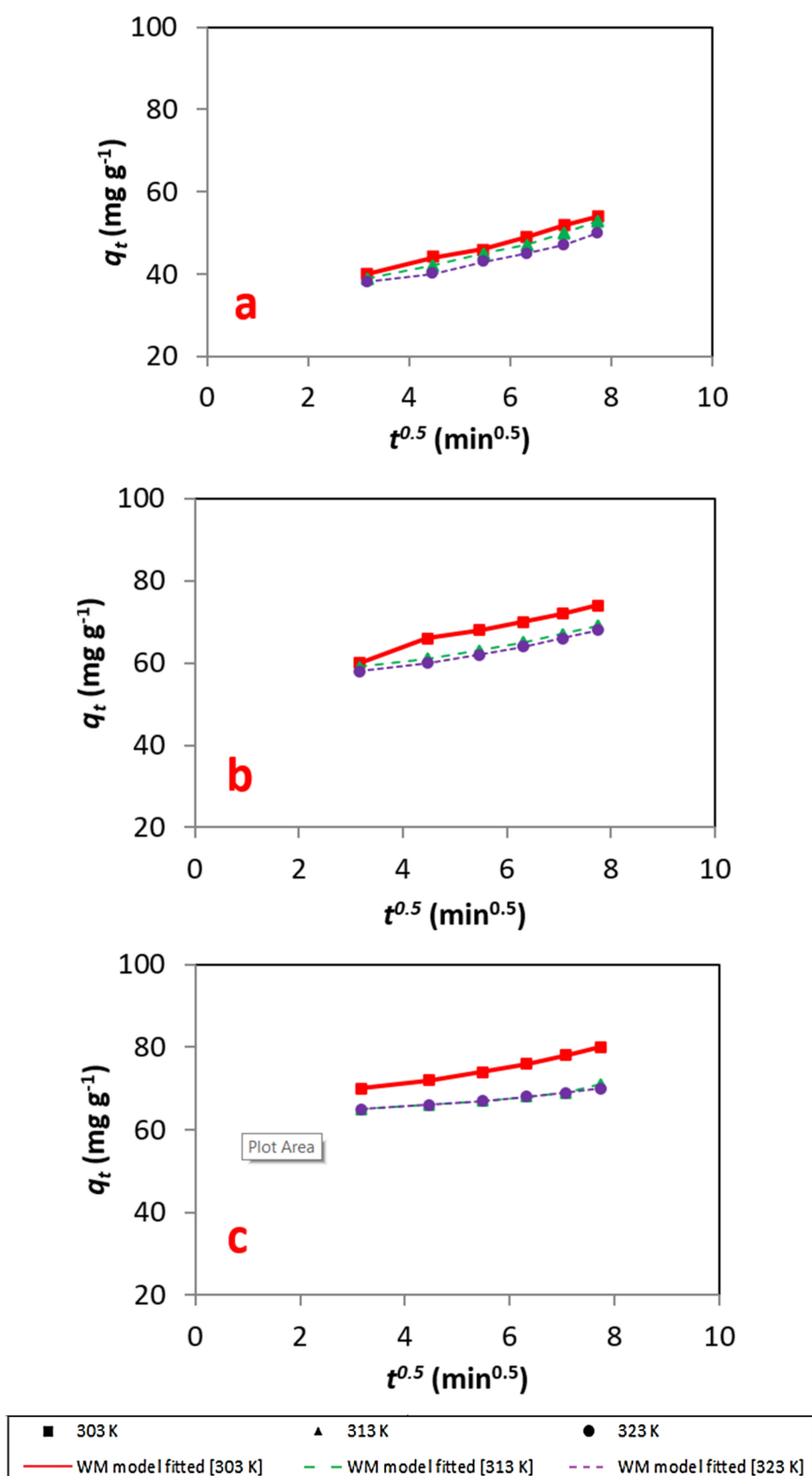| Initial Dye Concentration [μg mL^{-1}]	Temp [K]	$\Delta G°$ [kJ mol^{-1}]	$\Delta S°$ [J mol^{-1} K^{-1}]	$\Delta H°$ [kJ mol^{-1}]	ln A	E_a [kJ mol^{-1}]
100	303	−2.14				
	313	−2.19	3.39	2.04	0.86	9.66
	323	−2.31				
200	303	−1.22				
	313	−1.24	5.68	3.31	1.72	16.64
	323	−1.29				
300	303	−0.75				
	313	−0.81	8.73	4.80	4.07	32.36
	323	−0.87				

Figure 10. (**a–c**) Energy information fitted to the to the Weber–Morris model at different concentrations.
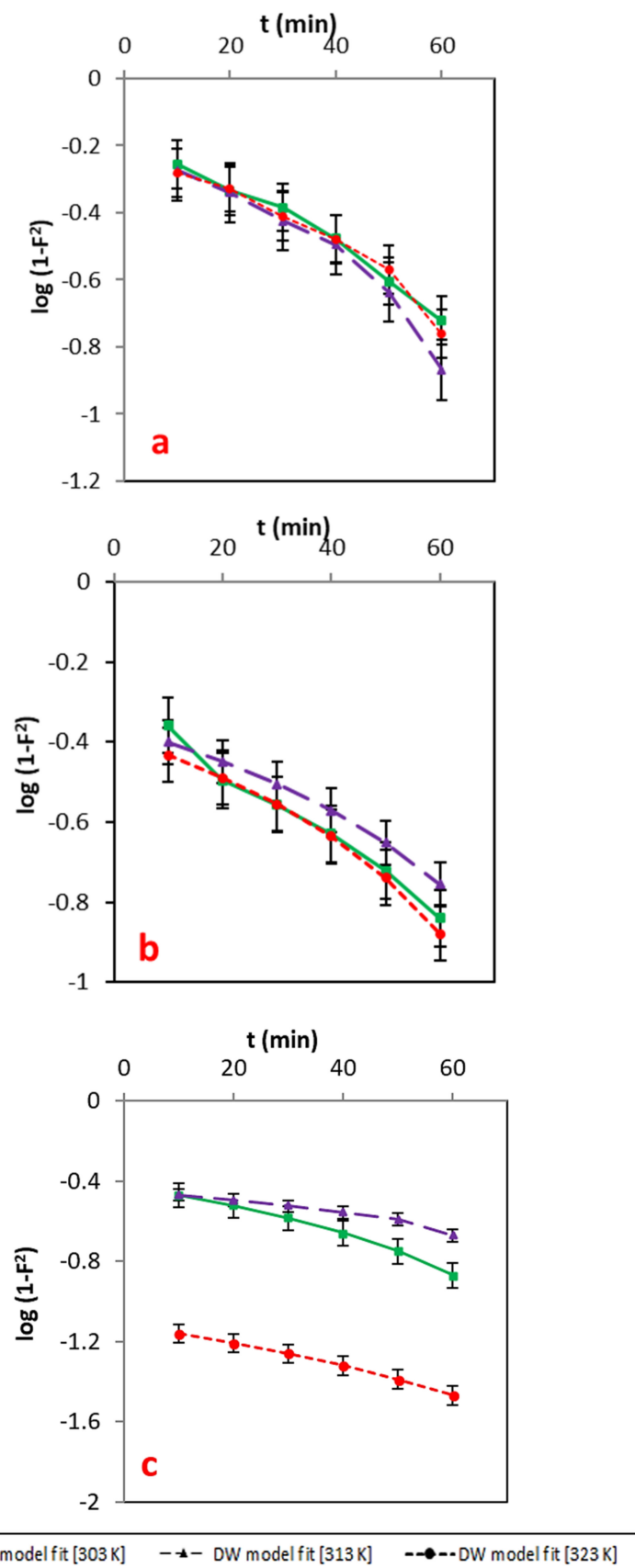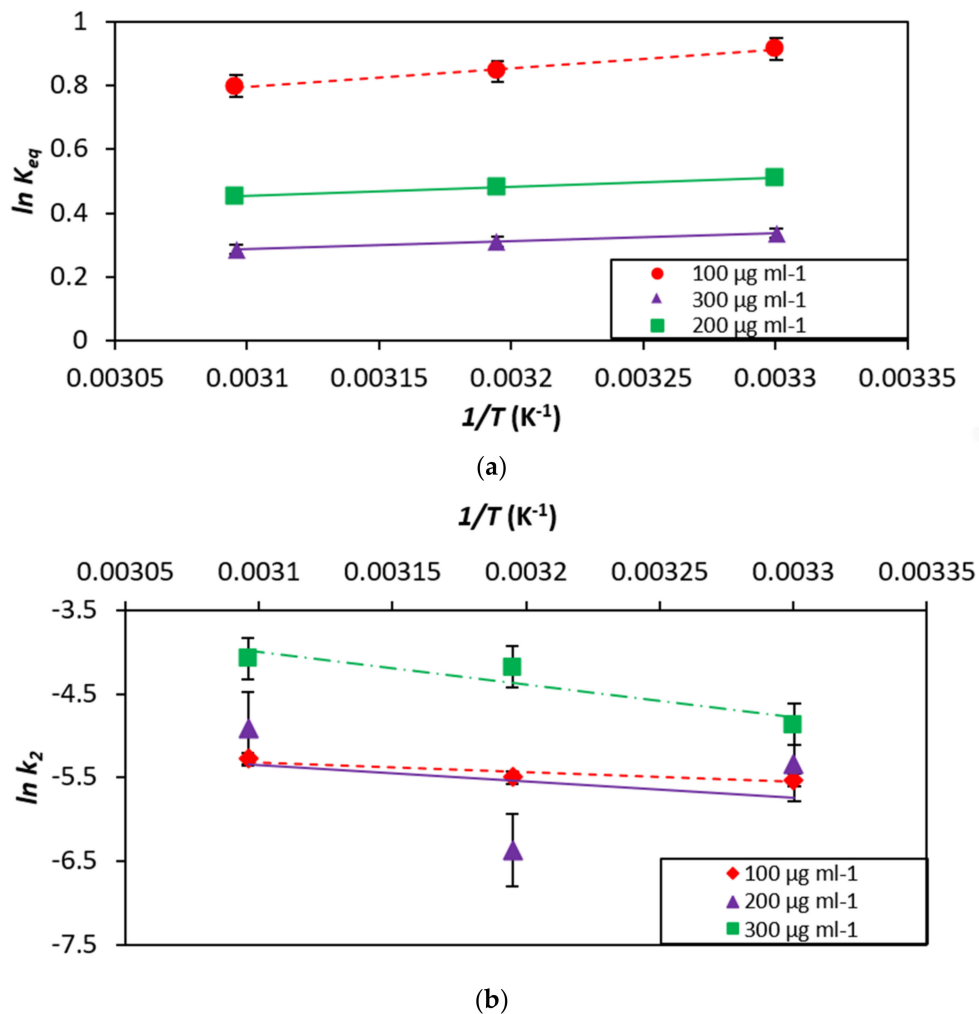
**Figure 11.** (**a–c**): Energy information fitted to the Dumwald–Wagner model at different concentrations.

(a)

(b)

Figure 12. (**a**) Determination of enthalpy and Gibbs free energy: plot of thermodynamic equilibrium constant against $1/T$ and (**b**) Determination of activation energy: plot of pseudo-second order kinetic constant against $1/T$.

3.7. Statistical Process Optimization

The process optimization was conducted using fractional factorial experimental design (FFED) under various combinations of five self-determining variables. The FEED analysis and the quadratic regression eq. obtained from ANOVA illustrate the probable specifics and combined effect of the factors for the DB15–HNT system [39–45]. For the ANOVA analysis, the *p*-value < 0.05% with 95% assurance span was considered noteworthy [44–50].

The graphs in Figure 13 represent a strong correlation between the particle data and the responses calculated with the FFED model. In addition, A, C, D, A^2, C^2, D^2, and E^2 are considerable model conditions for the DB15–HNT system. The regression Equation (1) obtained for DB15–HNT system is shown below:

$$\text{Response}_{\text{DB15-HNT}} = 42.1 + 18.5 \times A - 6.2 \times B + 19.5 \times C - 32.0 \times D - 13.4 \times E - 3.4 \times AB + 11.8 \times AC - 3.0 \times BC - 19.8 \times A^2 + 1.6 \times B^2 - 27.5 \times C^2 + 24.2 \times D^2 + 23.4 \times E^2 \quad (1)$$
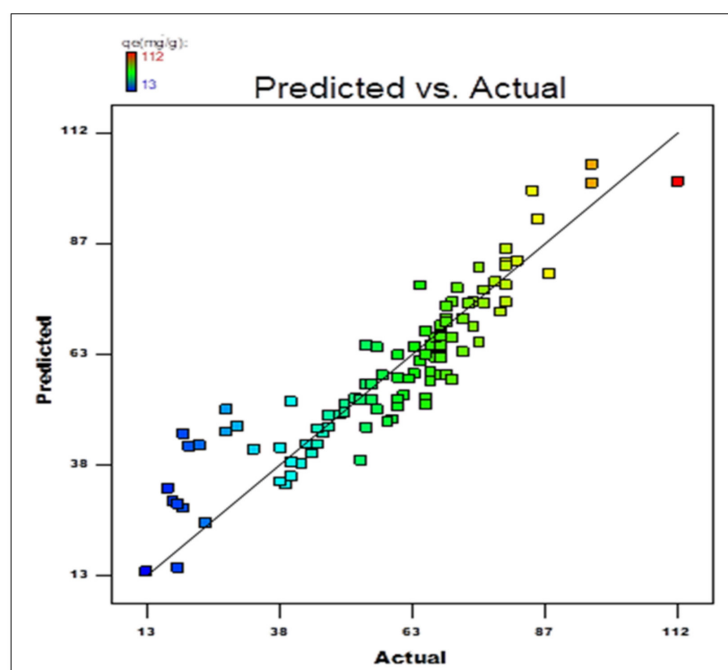
Figure 13. The calculated response against the experimental value obtained for adsorption capacity of DB15–HNT.

The regression coefficient [51–63] indicates the effect of various features affecting the adsorption capacity on the adsorption capacity [64–67]. The surface and contour plots represented in Figure 14 show the combined effect of two features on the process of adsorption. Statistical optimization experiment was 112 mg g^{-1} with conditions optimized pH = 1, the adsorbent dosage of 0.5 g L^{-1}, and an initial dye concentration of 412 mg L^{-1} for an adsorption time of 177 min with orbital shaking of 165 rpm at temperature 20 °C.

3.8. Adsorption Process for Textile Industrial Effluents

To measure the real-life performance of the prepared DB15, it was utilized to treat an industrial textile effluent (TIE) [66]. 0.1% (*w/v*) DB15 color arrangements were ready by dissolving 5 g of the color in 5L refined water (referred to as solution 1) and in 5 L TIE (referred to as Solution 2). Preliminary investigations were carried out to evaluate the effective parameters derived from optimization on the efficiency of the dye using aqueous matrices. It was observed that the addition of fresh samples at short intervals showed an effective treatment such that the adsorbent could amputate the dye along with the allied materials present in Solution 2.
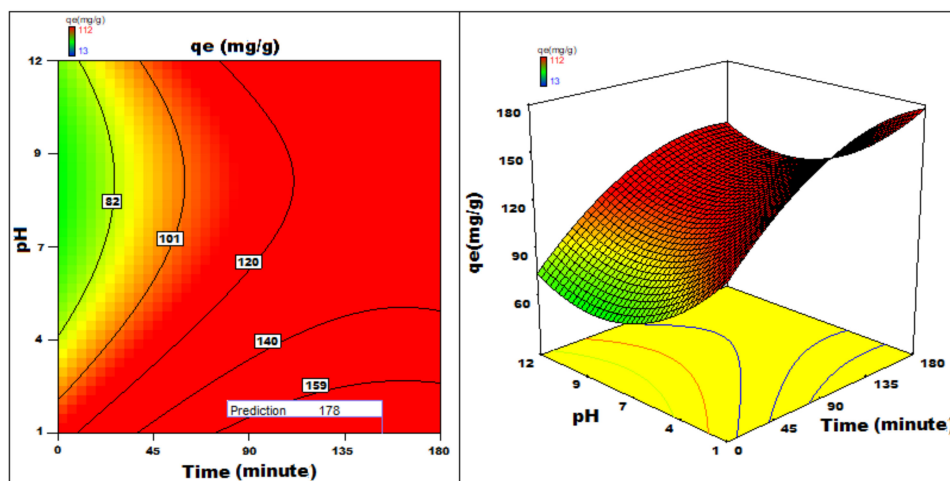
Figure 15 shows a visual comparison between distilled water, DB15 color in refined water, TIE arrangement, DB15 in TIE arrangement, and filtrate after the adsorption of color on HNT after 15 min.
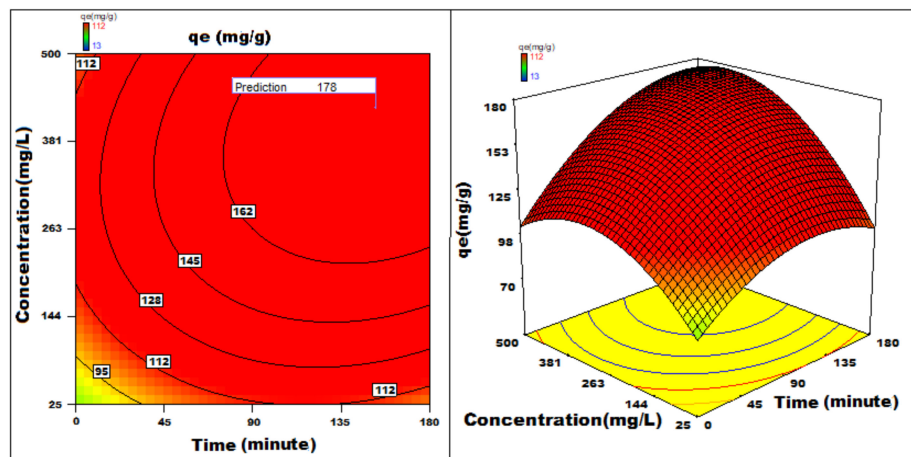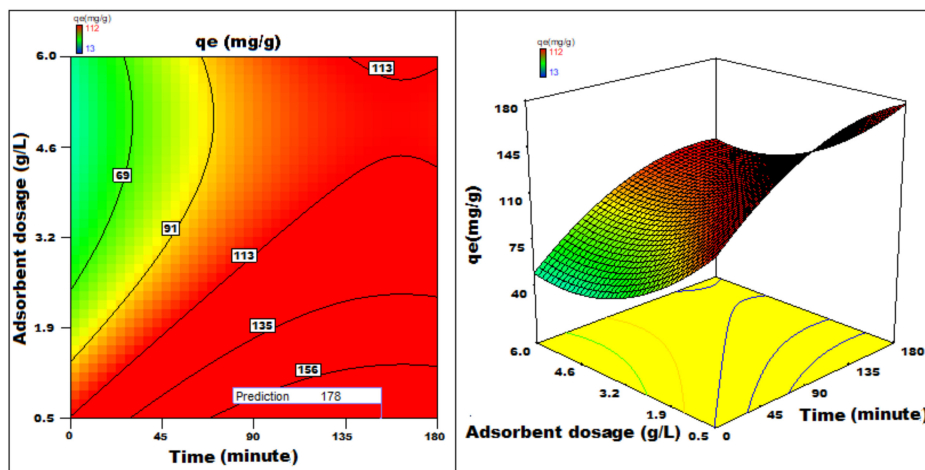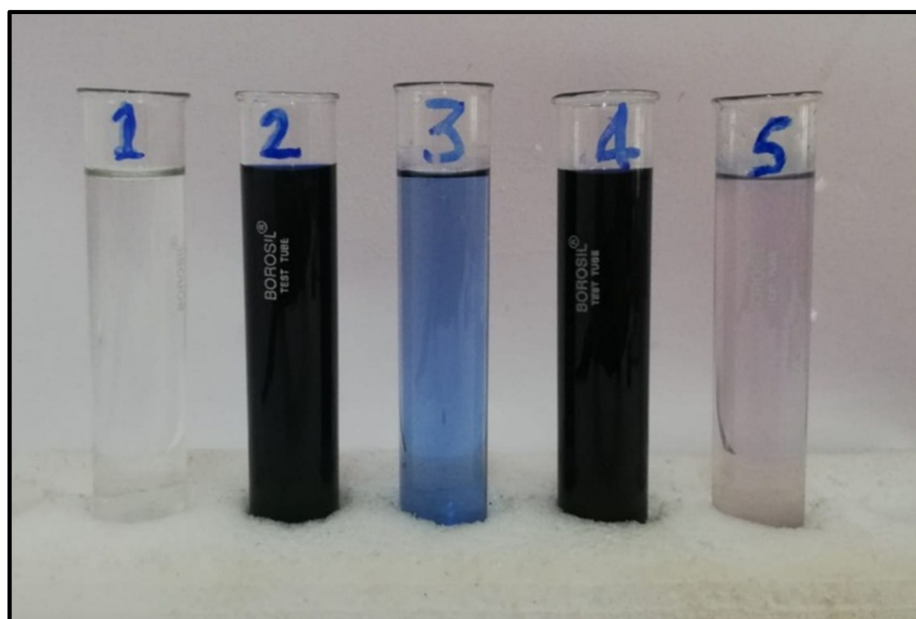
Figure 14. (**a**–**c**) 3D-surface plots and 2D-contour plots of variation of adsorption capacity with different parameters.

Figure 15. (1) Distilled water; (2) DB15 dye in distilled water; (3) TIE; (4) DB15 dye in TIE; (5) Filtrate after adsorption of dye on HNT after 15 min.

To scale up the experiments by one and two orders, 0.5 and 5.0 g each of the HNT was transferred to 1L and 10L polyethylene beakers. Next, 500 mL and 5 L Solution 2 was added to 1 L and 10L polyethylene beakers, respectively. Using a magnetic stirrer, the solutions were agitated. The procedure was repeated as described earlier [64–67].

4. Conclusions

The adsorption process is a dynamic phenomenon, and various factors seem to influence the remediation process synergistically. The study sets a new roadmap for the applied science by amalgamating the experimental analysis with in-depth modeling for an effective outcome. The connections among HNT as the adsorbent and DB15 color as the adsorbate displayed a test harmony (q_e) worth 96.00 mg g^{-1} at pH 2, 69.00 mg g^{-1} at a practically unbiased pH, and 112 mg g^{-1}, which was obtained via statistical optimization. To further understand the process of adsorption, nine isotherm models were studied. The adsorption follows Brouers–Sotolongo model, and the interactions between HNT and DB15 were identified to be physical in nature, following the pseudo-second-order kinetics. The contact time, dye concentration and dosage, and initial pH were the effective operating parameters influencing the adsorption. Based on the positive outcomes of the statistical optimization studies, the current work was tested at a laboratory scale for the application perspective. It was also demonstrated that the dye modified HNT has the potential to treat effluents from the textile industry. Furthermore, the current case study of the DB15 dye being adsorbed on the lucrative halloysite nanotubes sets a benchmark for remediation. Any given dye can be tested for its remediation purpose by choosing adsorbate material such as HNT. It would lead to a sustainable approach for tackling the current market demands. This study further bolsters the adsorption process by concretizing the need for modeling studies right from the laboratory scale to an industrial scale for process optimization. Thus, the work attracts researchers from various fields to address the current social/market needs by implementing green chemistry and green engineering principles for a sustainable environment.

Author Contributions: Conceptualization, S.J.U., M.R.S., M.N.A. and M.E.M.S.; methodology, S.J.U. and P.P.; software, S.J.U. and S.N.T.; validation, M.N.A., S.J.U. and U.T.S.; formal analysis, M.A.A. and R.A.M.; investigation, U.T.S. and R.A.M.; resources, M.I.H.S. and M.E.M.S.; data curation, M.E.M.S.; writing—original draft preparation, P.P. and S.J.U.; writing—review and editing, H.M.A. and A.E.;

References

1. Taqui, S.N.; Yahya, R.; Hassan, A.; Nayak, N.; Syed, A.A. A novel sustainable design to develop polypropylene and unsatu-rated polyester resin polymer composites from waste of major polluting industries and investigation on their physicomechan-ical and wear properties. *Polym. Compos.* **2019**, *40*, 1142–1157. [CrossRef]
2. Li, Y.; Lu, L.; Tan, Y.; Wang, L.; Shen, M. Decoupling Water Consumption and Environmental Impact on Textile Industry by Using Water Footprint Method: A Case Study in China. *Water* **2017**, *9*, 124. [CrossRef]
3. Püntener, A.; Page, C. European Ban on Certain Azo Dyes, Quality & Environment. *Eur. J.* **2004**, *14*, 231–458.
4. Kandelbauer, A.; Guebitz, G.M. Bioremediation for the Decolorization of Textile Dyes—A Review. *Environ. Chem.* **2005**, 269–288. [CrossRef]
5. Robinson, T.; McMullan, G.; Marchant, R.; Nigam, P. Remediation of dyes in textile effluent: A critical review on current treatment technologies with a proposed alternative. *Bioresour. Technol.* **2001**, *77*, 247–255. [CrossRef]
6. Anku, W.W.; Agorku, E.S.; Oppong, S.O.-B.; Karikari, A.Y. Mwcnts attached neodymium doped-ZnOphotocatalysts for efficient removal of dyes from wastewater. *SN Appl. Sci.* **2020**, *2*, 1–13. [CrossRef]
7. Ullah, I.; Ali, S.; Hanif, M.A.; Shahid, S.A. Nanoscience for environmental remediation: A review. *Int. J. Chem. Biochem. Sci.* **2012**, *2*, 60–77.
8. Kheddo, A.; Rhyman, L.; Elzagheid, M.I.; Jeetah, P.; Ramasami, P. Adsorption of synthetic dyed wastewater using activated carbon from rice husk. *SN Appl. Sci.* **2020**, *2*, 1–14. [CrossRef]
9. Strapasson, G.B.; Scheffer, F.R.; Cendron, S.W.; Silva, F.D.C.; Lazzari, N.H.; Azambuja, C.; Peyrot, A.; Weibel, D.E. Visible light sensitization of TiO$_2$/Ag/N nanostructures synthesized by microwave irradiation for oxidative degradation of organic dyes. *SN Appl. Sci.* **2020**, *2*, 1–12. [CrossRef]
10. Papegowda, P.K.; Syed, A.A. Isotherm, Kinetic and Thermodynamic Studies on the Removal of Methylene Blue Dye from Aqueous Solution Using Saw Palmetto Spent. *Int. J. Environ. Res.* **2017**, *11*, 91–98. [CrossRef]
11. Demirbas, A. Agricultural based activated carbons for the removal of dyes from aqueous solutions: A review. *J. Hazard. Mater.* **2009**, *167*, 1–9. [CrossRef]
12. Gupta, V.K.; Kumar, R.; Nayak, A.; Saleh, T.A.; Barakat, M.A. Adsorptive removal of dyes from aqueous solution onto carbon nanotubes: A review. *Adv. Colloid Interface Sci.* **2013**, *193*, 24–34. [CrossRef]
13. Garrido-Ramírez, E.G.; Theng, B.K.; Mora, M.L. Clays and oxide minerals as catalysts and nanocatalysts in Fenton-like reactions—A review. *Appl. Clay Sci.* **2010**, *47*, 182–192. [CrossRef]
14. Carretero, M.I.; Pozo, M. Clay and non-clay minerals in the pharmaceutical and cosmetic industries Part II. Active ingredients. *Appl. Clay Sci.* **2010**, *47*, 171–181. [CrossRef]
15. Ambre, A.H.; Katti, K.S.; Katti, D. Nanoclay Based Composite Scaffolds for Bone Tissue Engineering Applications. *J. Nanotechnol. Eng. Med.* **2010**, *1*, 031013. [CrossRef]
16. Vinokurov, V.; Novikov, A.; Rodnova, V.; Anikushin, B.; Kotelev, M.; Ivanov, E.; Lvov, Y. Cellulose Nanofibrils and Tubular Halloysite as Enhanced Strength Gelation Agents. *Polymers* **2019**, *11*, 919. [CrossRef] [PubMed]
17. Chequer, F.D.; de Oliveira, G.R.; Ferraz, E.A.; Cardoso, J.C.; Zanoni, M.B.; de Oliveira, D.P. Textile dyes: Dyeing process and environmental impact. In *Eco-Friendly Textile Dyeing and Finishing*; IntechOpen: London, UK, 2013; Volume 6, pp. 151–176.
18. Sanghi, R.; Bhattacharya, B. Review on decolorisation of aqueous dye solutions by low cost adsorbents. *Color. Technol.* **2002**, *118*, 256–269. [CrossRef]
19. Sulthana, R.; Taqui, S.N.; Zameer, F.; Syed, U.T.; Syed, A.A. Adsorption of ethidium bromide from aqueous solution onto nutraceutical industrial fennel seed spent: Kinetics and thermodynamics modeling studies. *Int. J. Phytoremediat.* **2018**, *20*, 1075–1086. [CrossRef]

20. Taqui, S.N.; Yahya, R.; Hassan, A.; Nayak, N.; Syed, A.A. Adsorption of Acid Blue 113 from aqueous solution onto nutraceutical industrial coriander seed spent: Isotherm, kinetics, thermodynamics and modeling studies. *Desalin. Water Treat.* **2019**, *153*, 321–337. [CrossRef]

21. Taqui, S.N.; Yahya, R.; Hassan, A.; Nayak, N.; Syed, A.A. Development of sustainable dye adsorption system using nutraceutical industrial fennel seed spent—studies using Congo red dye. *Int. J. Phytoremediat.* **2017**, *19*, 686–694. [CrossRef] [PubMed]

22. Allah, M.A.H.D.; Taqui, S.N.; Syed, U.T.; Syed, A.A. Development of sustainable acid blue 113 dye adsorption system using nutraceutical industrial Tribulusterrestris spent. *SN Appl. Sci.* **2019**, *1*, 330. [CrossRef]

23. Childress, A.E.; Elimelech, M. Effect of solution chemistry on the surface charge of polymeric reverse osmosis and nanofiltra-tion membranes. *J. Membr. Sci.* **1996**, *119*, 253–268. [CrossRef]

24. Baral, S.; Das, N.; Chaudhury, G.R.; Das, S. A preliminary study on the adsorptive removal of Cr (VI) using seaweed, *Hydrilla verticillata*. *J. Hazard. Mater.* **2009**, *171*, 358–369. [CrossRef] [PubMed]

25. Alkan, M.; Demirbaş, Ö.; Doğan, M. Adsorption kinetics and thermodynamics of an anionic dye onto sepiolite. *Microporous Mesoporous Mater.* **2007**, *101*, 388–396. [CrossRef]

26. Langmuir, I. The constitution and fundamental properties of solids and liquids. Part I. Solids. *J. Am. Chem. Soc.* **1916**, *38*, 2221–2295. [CrossRef]

27. Freundlich, H. Over the adsorption in solution. *J. Phys. Chem.* **1906**, *57*, 1100–1107.

28. Jovanović, D.S. Physical adsorption of gases. *Colloid Polym. Sci.* **1969**, *235*, 1214–1225. [CrossRef]

29. Dubinin, M. The equation of the characteristic curve of activated charcoal. *Proc. USSR Acad. Sci.* **1947**, *55*, 327–329.

30. Yakutha, S.A.; Taquib, S.N.; Syedc, U.T.; Syeda, A.A. Nutraceutical industrial chillies stalk waste as a new adsorbent for the removal of Acid Violet 49 from water and textile industrial effluent: Adsorption isotherms and kinetic models. *Desalin. Water Treat.* **2019**, *155*, 94–112. [CrossRef]

31. Toth, J. State equation of the solid-gas interface layers. *Acta Chim. Hung.* **1971**, *69*, 311–328.

32. Brouers, F.; Sotolongo-Costa, O.; Marquez, F.; Pirard, J.-P. Microporous and heterogeneous surface adsorption isotherms arising from Levy distributions. *Phys. A Stat. Mech. Its Appl.* **2005**, *349*, 271–282. [CrossRef]

33. Vieth, W.; Sladek, K. A model for diffusion in a glassy polymer. *J. Colloid Sci.* **1965**, *20*, 1014–1033. [CrossRef]

34. Radke, C.J.; Prausnitz, J.M. Adsorption of Organic Solutes from Dilute Aqueous Solution of Activated Carbon. *Ind. Eng. Chem. Fundam.* **1972**, *11*, 445–451. [CrossRef]

35. Redlich, O.; Peterson, D.L. A Useful Adsorption Isotherm. *J. Phys. Chem.* **1959**, *63*, 1024. [CrossRef]

36. Lagergren, S.K. About the theory of so-called adsorption of soluble substances. *Sven. Vetenskapsakad. Handingarl* **1898**, *24*, 1–39.

37. Ho, Y.-S.; McKay, G. Sorption of dye from aqueous solution by peat. *Chem. Eng. J.* **1998**, *70*, 115–124. [CrossRef]

38. Boyd, E.G.; Adamson, W.A.; Myers, S.L., Jr. The exchange adsorption of ions from aqueous solutions by organic zeolites. II. Kinetics[1]. *J. Am. Chem. Soc.* **1947**, *69*, 2836–2848. [CrossRef]

39. Wang, H.-L.; Chen, J.-L.; Zhai, Z.-C. Study on thermodynamics and kinetics of adsorption of p-toluidine from aqueous solu-tion by hypercrosslinked polymeric adsorbents. *Environ. Chem.-Beijing* **2004**, *23*, 192–196.

40. Taqui, S.N.; Yahya, R.; Hassan, A.; Khanum, F.; Syed, A.A. Valorization of Nutraceutical Industrial Coriander Seed Spent by the Process of Sustainable Adsorption System of Acid Black 52 from Aqueous Solution. *Int. J. Environ. Res.* **2019**, *13*, 639–659. [CrossRef]

41. Shahsavar, A.; Khanmohammadi, S.; Karimipour, A.; Goodarzi, M. A novel comprehensive experimental study concerned synthesizes and prepare liquid paraffin-Fe_3O_4 mixture to develop models for both thermal conductivity & viscosity: A new approach of GMDH type of neural network. *Int. J. Heat Mass Transf.* **2019**, *131*, 432–441. [CrossRef]

42. Jiang, Y.; Bahrami, M.; Bagherzadeh, S.A.; Abdollahi, A.; Sulgani, M.T.; Karimipour, A.; Goodarzi, M.; Bach, Q.-V. Propose a new approach of fuzzy lookup table method to predict Al_2O_3/deionized water nanofluid thermal conductivity based on achieved empirical data. *Phys. A Stat. Mech. Its Appl.* **2019**, *527*, 121177. [CrossRef]

43. Liu, W.; Malekahmadi, O.; Bagherzadeh, S.A.; Ghashang, M.; Karimipour, A.; Hasani, S.; Tlili, I.; Goodarzi, M. A novel comprehensive experimental study concerned graphene oxide nanoparticles dispersed in water: Synthesise, characterisation, thermal conductivity measurement and present a new approach of R87847LSF neural network. *Int. Commun. Heat Mass Transf.* **2019**, *109*, 104333. [CrossRef]

44. Farade, R.A.; Wahab, N.I.B.A.; Mansour, D.E.A.; Azis, N.B.; Jasni, J.; Banapurmath, N.R.; Soudagar, M.E.M. Investigation of the dielectric and thermal properties of non-edible cottonseed oil by infusing h-BN nanoparticles. *IEEE Access* **2020**, *8*, 76204–76217. [CrossRef]

45. Yaradoddi, J.S.; Banapurmath, N.R.; Ganachari, S.V.; Soudagar, M.E.M.; Mubarak, N.M.; Hallad, S.; Hugar, S.; Fayaz, H. Biodegradable carboxymethyl cellulose based material for sustainable packaging application. *Sci. Rep.* **2020**, *10*, 1–13. [CrossRef] [PubMed]

46. Ahmed, W.; Kazi, S.N.; Chowdhury, Z.Z.; Johan, M.R.B.; Soudagar, M.E.M.; Mujtaba, M.A.; Gul, M.; Badruddin, I.A.; Kamangar, S. Ultrasonic assisted new Al2O3@ TiO2-ZnO/DW ternary composites nanofluids for enhanced energy transportation in a closed horizontal circular flow passage. *Int. Commun. Heat Mass Transf.* **2021**, *120*, 105018. [CrossRef]

47. Peng, Y.; Khaled, U.; Al-Rashed, A.A.; Meer, R.; Goodarzi, M.; Sarafraz, M. Potential application of Response Surface Methodology (RSM) for the prediction and optimization of thermal conductivity of aqueous CuO (II) nanofluid: A statistical approach and experimental validation. *Phys. A Stat. Mech. Its Appl.* **2020**, *554*, 124353. [CrossRef]

48.   Wu, H.; Bagherzadeh, S.A.; D'Orazio, A.; Habibollahi, N.; Karimipour, A.; Goodarzi, M.; Bach, Q.-V. Present a new multi objective optimization statistical Pareto frontier method composed of artificial neural network and multi objective genetic algorithm to improve the pipe flow hydrodynamic and thermal properties such as pressure drop and heat transfer coefficient for non-Newtonian binary fluids. *Phys. A Stat. Mech. Its Appl.* **2019**, *535*, 122409. [CrossRef]

49.   Ghasemi, A.; Hassani, M.; Goodarzi, M.; Afrand, M.; Manafi, S. Appraising influence of COOH-MWCNTs on thermal conductivity of antifreeze using curve fitting and neural network. *Phys. A Stat. Mech. Its Appl.* **2019**, *514*, 36–45. [CrossRef]

50.   Afzal, A.; Khan, S.A.; Islam, M.T.; Jilte, R.D.; Khan, A.; Soudagar, M.E.M. Investigation and back-propagation modeling of base pressure at sonic and supersonic Mach numbers. *Phys. Fluids* **2020**, *32*, 096109. [CrossRef]

51.   Farade, R.A.; Abdul Wahab, N.I.; Mansour, D.E.A.; Azis, N.B.; Soudagar, M.E.M.; Siddappa, V. Development of Graphene Oxide-Based Nonedible Cottonseed Nanofluids for Power Transformers. *Materials* **2020**, *13*, 2569. [CrossRef]

52.   Giwa, S.O.; Sharifpur, M.; Goodarzi, M.; Alsulami, H.; Meyer, J.P. Influence of base fluid, temperature, and concentration on the thermophysical properties of hybrid nanofluids of alumina–ferrofluid: Experimental data, modeling through enhanced ANN, ANFIS, and curve fitting. *J. Therm. Anal. Calorim.* **2021**, *143*, 4149–4167. [CrossRef]

53.   Karimipour, A.; Bagherzadeh, S.A.; Goodarzi, M.; Alnaqi, A.A.; Bahiraei, M.; Safaei, M.R.; Shadloo, M.S. Synthesized $CuFe_2O_4/SiO_2$ nanocomposites added to water/EG: Evaluation of the thermophysical properties beside sensitivity analysis & EANN. *Int. J. Heat Mass Transf.* **2018**, *127*, 1169–1179. [CrossRef]

54.   Peng, Y.; Parsian, A.; Khodadadi, H.; Akbari, M.; Ghani, K.; Goodarzi, M.; Bach, Q.-V. Develop optimal network topology of artificial neural network (AONN) to predict the hybrid nanofluids thermal conductivity according to the empirical data of Al_2O_3-Cu nanoparticles dispersed in ethylene glycol. *Phys. A Stat. Mech. Its Appl.* **2020**, *549*, 124015. [CrossRef]

55.   Ahmadi, M.H.; Mohseni-Gharyehsafa, B.; Ghazvini, M.; Goodarzi, M.; Jilte, R.; Kumar, R. Comparing various machine learning approaches in modeling the dynamic viscosity of CuO/water nanofluid. *J. Therm. Anal. Calorim.* **2019**, *139*, 2585–2599. [CrossRef]

56.   Alrashed, A.A.; Akbari, O.A.; Heydari, A.; Toghraie, D.; Zarringhalam, M.; Shabani, G.A.S.; Seifi, A.R.; Goodarzi, M. The numerical modeling of water/FMWCNT nanofluid flow and heat transfer in a backward-facing contracting channel. *Phys. B Condens. Matter* **2018**, *537*, 176–183. [CrossRef]

57.   Alrashed, A.A.; Gharibdousti, M.S.; Goodarzi, M.; de Oliveira, L.R.; Safaei, M.R.; Filho, E.B. Effects on thermophysical properties of carbon based nanofluids: Experimental data, modelling using regression, ANFIS and ANN. *Int. J. Heat Mass Transf.* **2018**, *125*, 920–932. [CrossRef]

58.   Bahrami, M.; Akbari, M.; Bagherzadeh, S.A.; Karimipour, A.; Afrand, M.; Goodarzi, M. Develop 24 dissimilar ANNs by suitable architectures & training algorithms via sensitivity analysis to better statistical presentation: Measure MSEs between targets & ANN for Fe-CuO/Eg–Water nanofluid. *Phys. A Stat. Mech. Its Appl.* **2019**, *519*, 159–168. [CrossRef]

59.   Hossain, N.; Mahlia, T.M.I.; Miskat, M.I.; Chowdhury, T.; Barua, P.; Chowdhury, H.; Nizamuddin, S.; Ahmad, N.B.; Zaharin, N.A.B.; Mazari, S.A.; et al. Bioethanol production from forest residues and life cycle cost analysis of bioethanol-gasoline blend on transportation sector. *J. Environ. Chem. Eng.* **2021**, *9*, 105542. [CrossRef]

60.   Ahmed, W.; Kazi, S.N.; Chowdhury, Z.Z.; Johan, M.R.B.; Mehmood, S.; Soudagar, M.E.M.; Mujtaba, M.A.; Gul, M.; Ahmad, M.S. Heat transfer growth of sonochemically synthesized novel mixed metal oxide ZnO+ Al2O3+ TiO2/DW based ternary hybrid nanofluids in a square flow conduit. *Renew. Sustain. Energy Rev.* **2021**, *145*, 111025. [CrossRef]

61.   Ahmed, W.; Chowdhury, Z.Z.; Kazi, S.N.; Johan, M.R.B.; Abdelrazek, A.H.; Fayaz, H.; Badruddin, I.; Mujtaba, M.A.; Soudagar, M.E.M.; Akram, N.; et al. Experimental evaluation and numerical verification of enhanced heat transportation by using ultrasonic assisted nanofluids in a closed horizontal circular passage. *Case Stud. Therm. Eng.* **2021**, *26*, 101026. [CrossRef]

62.   Shahapurkar, K.; Chenrayan, V.; Soudagar, M.E.M.; Badruddin, I.A.; Shahapurkar, P.; Elfasakhany, A.; Mujtaba, M.A.; Siddiqui, M.I.H.; Ali, M.A.; Mahlia, T.M.I. Leverage of Environmental Pollutant Crump Rubber on the Dry Sliding Wear Response of Epoxy Composites. *Polymers* **2021**, *13*, 2894. [CrossRef]

63.   Usman, M.; Hussain, H.; Riaz, F.; Irshad, M.; Bashir, R.; Shah, M.H.; Zafar, A.A.; Bashir, U.; Kalam, M.A.; Mujtaba, M.A.; et al. Artificial Neural Network Led Optimization of Oxyhydrogen Hybridized Diesel Operated Engine. *Sustainability* **2021**, *13*, 9373. [CrossRef]

64.   Taqui, S.N.; Mohan, C.S.; Khatoon, B.A.; Soudagar, M.E.M.; Khan, T.M.; Mujtaba, M.A.; Ahmed, W.; Elfasakhany, A.; Kumar, R.; Pruncu, C.I. Sustainable adsorption method for the remediation of malachite green dye using nutraceutical industrial fenugreek seed spent. *Biomass Convers. Biorefinery* **2021**, 12. [CrossRef]

65.   Taqui, S.N.; Mohan, C.S.; Goodarzi, M.S.; Elkotb, M.A.; Khatoon, B.A.; Soudagar, M.E.M.; Koki, I.B.; Elfasakhany, A.; Khalifa, A.S.; Ali, M.A.; et al. Sustainable Adsorption Method for the Remediation of Crystal Violet Dye Using Nutraceutical Industrial Fenugreek Seed Spent. *Appl. Sci.* **2021**, *11*, 7635. [CrossRef]

66.   Dhaif-Allah, M.A.H.; Taqui, S.N.; Syed, U.T.; Syed, A.A. Kinetic and isotherm modeling for acid blue 113 dye adsorption onto low-cost nutraceutical industrial fenugreek seed spent. *Appl. Water Sci.* **2020**, *10*, 1–16. [CrossRef]

67.   Ukkund, S.J.; Puthiyillam, P.; Alshehri, H.M.; Goodarzi, M.; Taqui, S.N.; Anqi, A.E.; Safaei, M.R.; Ali, M.A.; Syed, U.T.; Mir, R.A.; et al. Adsorption Method for the Remediation of Brilliant Green Dye Using Halloysite Nanotube: Isotherm, Kinetic and Modeling Studies. *Appl. Sci.* **2021**, *11*, 8088. [CrossRef]